STUDIES OF AIRCRAFT FLOW FIELDS AT INLET LOCATIONS

by

Lyndell S.King* and Terence W.Schmidt†

*Ames Research Center, NASA
Moffett Field, California, U.S.A., 94035

†Arnold Research Organization, Inc.
Ames Division
Moffett Field, California, U.S.A., 94035

SUMMARY

Results are presented from a wind-tunnel investigation of the flow fields about fuselage configurations at transonic and supersonic speeds ($0.8 \leqslant M_\infty \leqslant 2.5$) and at angles of attack up to 24°. A family of seven fuselages with different cross-sectional shapes was tested in conjunction with two nose shapes, two canopies, and two wings of different sweep. Flow-field surveys were performed at two likely inlet locations – ahead of and under the wing – to assess the effects of forebody geometry throughout the Mach number and angle-of-attack envelope.

Flow-field results are presented as contour maps of the local values of Mach number, total pressure, and flow angularities in the two survey planes. Comparisons are made to illustrate the effects of Mach number, angle of attack, and forebody variations. Comparisons are also made of the results with predictions using the numerical method of Walitt, et al.

The experimental data particularly indicate the strong influence of the canopy, nose droop, and fuselage shape on flow angularities in the forward survey plane. Nose droop and the canopy both tend to reduce sensitivity to positive angles of attack and to reduce the extent of influence of fuselage lower corner geometry. Under the wing, however, the flow field is dominated by the effects of the wing itself.

STUDIES OF AIRCRAFT FLOW FIELDS AT INLET LOCATIONS

Lyndell S. King*
Ames Research Center, NASA
Moffett Field, California, U. S. A., 94035

and

Terrence W. Schmidt**
Arnold Research Organization, Inc.
Ames Division
Moffett Field, California, U. S. A., 94035

1. Introduction

Requirements for higher flight Mach numbers and greater maneuverability of aircraft impose greater difficulties in obtaining satisfactory inlet performance over the operating envelope. Since the inlet must operate within the flow environment generated by the aircraft, inlet-airframe integration effects assume major importance because of sensitivity of inlets and engines to angularity and nonuniformity of the entering flow. The flow field upstream of inlets must therefore be adequately described, and, in particular, the effects of vehicle geometry ahead of the inlet must be determined throughout the operating envelope.

The flow fields about fuselage and fuselage-wing configurations were therefore investigated in a wind tunnel at transonic and supersonic speeds. Objectives of the test program were to determine the flow fields around a family of fuselage-wing configurations representative of advanced tactical aircraft, and to determine body-wing-inlet interaction effects for inlets at various locations on the fuselage. The test program consisted of the following: (1) forebody (including wing stub) flow-field investigation; (2) inlet tests to determine the characteristics of isolated inlets; and (3) combined inlet-forebody investigation to determine interaction effects. This paper, however, is concerned only with results from the flow-field investigation.

2. Description of Models

The family of configurations tested was selected from recent and proposed tactical aircraft. The selections were meant to provide a limited study of the more significant forebody geometric variables: fuselage cross-sectional shape, nose shape, canopy profile, and wing sweep. The configuration shown in Fig. 1 illustrates the general arrangement of the body-wing components investigated. The models consisted of a basic and an alternate nose, canopy, and wing. Both noses were ogives drooped 7.5° relative to the fuselage horizontal reference line. The basic canopy was representative of single-seat aircraft, and the alternate canopy, of tandem seating. The basic wing was swept 55° and the alternate wing, 65°; otherwise they were identical.

A feature often desired in the design of tactical aircraft is a relatively large flat area on the lower surface of the fuselage for mounting external stores. This feature requires the lower fuselage corner to have a small radius. Thus two groups of fuselage shapes (Fig. 2) were selected to assess the effect of a flat bottom and the resulting short radius corner on the flow field at the inlet face. Configurations 1, 3, and 5 represent three variations of a corner with small radius, and the remaining four configurations are variations of a much more generous corner. The configurations within the two groups should provide an insight into the effects of corner geometry.

The model tested was approximately one-twelfth scale and consisted of a main fuselage member with several attachable components. These components – the two noses, two canopies, two wings, and seven lower fuselages – could be mounted in many possible combinations to represent different aircraft configurations.

3. Instrumentation and Test Description

The tests were performed in the Ames 6- by 6-Foot and the 8- by 7-Foot Wind Tunnels at Mach numbers from 0.8 to 2.5. Free-stream total pressure was maintained at 20 in. Hg during all the tests. Corresponding Reynolds numbers per foot were 2.88×10^6 at M = 0.8 and 1.98×10^6 at M = 2.5. Angles of attack ranged from -3° to 24°, and angles of sideslip, from -13° to 13°.

Instrumentation for the tests consisted of 72 forebody surface pressure taps and a rake of three movable conical probes. This instrumentation is illustrated in Fig. 3. Flow-field survey data were taken at two planes along the fuselage – at station 19.5 and at station 32.5 – corresponding to 30 and 50 percent of the aircraft length. These two locations, forward of the wing and under the wing, are representative of typical longitudinal inlet locations for tactical aircraft.

The flow-field probes were 0.125-inch maximum diameter cones with an included angle of 40°. Five orifices of 0.020-inch diameter were located on each cone; one at the nose to measure pitot pressure, and four on the conical surface spaced at 90° intervals. As shown in Fig. 3 the probes were mounted on a rake, which in turn was mounted on a drive mechanism. The mechanism was remotely controlled to move the probes in the two orthogonal directions in the survey plane. In addition, the angle of attack of the probes could be remotely varied to aline the rake roughly with the approaching flow and avoid exceeding the calibration limits of the conical probes.

4. Data Reduction and Accuracy

The calibration data obtained with the conical probes, and the five pressure measurements on each cone provided sufficient information for calculating the local Mach number, total pressure, and flow angularity for each probe location in the flow field. The data reduction procedure for the conical probes is identical to that in (1).

Data were taken at 30 points in the survey plane, corresponding to 10 positions of the conical probe rake. Because of the thousands of contour plots required to present all the flow-field data obtained in the test, it was considered desirable to automate the

*Research Scientist
**Research Engineer

data reduction to the extent that the computer would produce the contour plots. Such a map is shown in Fig. 4 along with the reduced test data from which it was generated.

In Fig. 4, note that errors are introduced in contouring the flow-field measurements. The contouring procedure uses a continuous approximating function, which may be partially advantageous in smoothing data scatter. However, for regions of high gradients, the accuracy is adversely affected. Gradients in the flow field increase with Mach number and with angle of attack; thus Fig. 4 showing fuselage 3 at a free-stream Mach number of 2.2 and an angle of attack of 20.75° is illustrative of the contouring accuracy expected under adverse conditions.

A question naturally arises at this point as to the accuracy of both the reduced test data and the contour plots. To gain some insight into the accuracy of the results, the possible sources of errors, of which there are many for a program of this type, should be considered. Errors may stem from nonuniformities in the wind-tunnel flow, from the alinement of the flow-field rake, from construction of the cones, and from the calibration curves for each of the cones. Efforts have been made to account for, and minimize, when possible, these errors. For example, corrections based on flow angularities in the wind tunnel have been applied to the data. However, it is not possible to quantify each error, so the combined effect from all sources must be examined to understand the total errors involved. Testing with the probe rake and drive mechanism alone in the wind tunnel will provide a basis for comparison of the flow conditions calculated from the probe measurements.

The results of such a comparison have been analyzed statistically, and the standard deviation of the reduced test data has been computed for each flow variable. The standard deviation is defined as the absolute value of the error within which 68 percent of the data is contained. For the reduced test data the standard deviation was found to be primarily a function of the Mach number. Standard deviations of the reduced test data at Mach numbers of 0.8 and 2.2 are shown in Table I along with the errors introduced in contouring the data and the combined errors from the two sources.

TABLE 1.– EXPERIMENTAL AND CONTOURING ERRORS

Variable	M_∞	α	Standard deviation		
			Experimental data	Contour	Total
p_{T_1}/p_{T_∞}	0.8	0°	0.001	0.0002	0.001
		15	.001	.0004	.001
	2.2	0	.020	.0060	.021
		15	.020	.0069	.021
		20.75	.020	.0198	.028
M_1	.8	0°	.006	.0016	.006
		15	.006	.0016	.006
	2.2	0	.012	.0060	.013
		15	.012	.0170	.021
		20.75	.012	.0398	.042
ϵ	.8	0°	.33°	.12°	.35°
		15	.33	.17	.37
	2.2	0	.67	.09	.68
		15	.67	.29	.73
		20.75	.67	.56	.87
σ	.8	0°	.40°	.06°	.40°
		15	.40	.09	.41
	2.2	0	.50	.15	.52
		15	.50	.25	.56
		20.75	.50	.92	1.05

5. Comparison with Numerical Results

It is of some interest to compare the experimental results with predictions from the numerical procedure of Walitt, Trulio, and King (2). This method is based on a time-dependent, two-dimensional numerical solution of the Navier-Stokes equations. By using the equivalence principle to relate the time dependence to the axial position along the body, the method provides an approximation to the steady, three-dimensional flow about a body of rather arbitrary cross-sectional shape at angle of attack. Because of the equivalence principle assumption, the method is limited to supersonic speeds. In addition, axial viscous effects are neglected, although viscous terms are included in the cross-flow calculations.

The numerical method has been used to compute the flow field characteristics about one of the configurations from the experimental program – fuselage 1 at a Mach number of 2.5 and 15° angle of attack. The computed results are presented in Fig. 5 and compared with the experimental results. Agreement between the predicted and experimental results is considered good, particularly in the lower quadrant of the flow field. Differences may be noted in the canopy shock location and in the flow field about the canopy. These differences result from the assumption of the equivalence principle, which neglects any perturbation of the axial velocities from the free-stream axial component of velocity. In general, it is felt that these comparisons lend credence to the numerical results.

6. Discussion of Experimental Results

Although this test program investigated in detail the flow-field effects due to Mach number, angle of attack, and fuselage forebody variations, only a small portion of the data is presented. That portion was selected to provide a general understanding of the flow-field characteristics and to illustrate trends in the change of flow-field characteristics associated with major component changes.

In Fig. 6 the effects of Mach number on the flow field at the forward inlet station are illustrated for fuselage 3 at 0° and 15° angle of attack. Data for $\alpha = 0°$ are on the left-hand side of the fuselage cross section. Maps of the local total pressure ratio are shown for $\alpha = 15°$, and local values of the downwash and sidewash angles are presented for both angles of attack. The downwash angle is

defined relative to the free-stream direction: for example, with the body at 15° angle of attack, a downwash angle of +3° corresponds to a local angle of attack of 12°. For zero flow inclination relative to the body, the corresponding downwash angle is 15°. Upwash is negative downwash and is referenced to the free-stream direction. The sidewash angles are defined as positive outward from the body.

Fig. 6 reveals some interesting flow-field characteristics. Looking first at the flow angularity maps for 0° angle of attack we see that changes in the flow field are relatively insignificant at the lower Mach numbers but increase with Mach number. Because of the nose droop, the fuselage is effectively at a negative angle of attack. The drooped nose and the canopy combine to give the flow a net downwash, an effect particularly apparent at $M_\infty = 2.2$. Also it is noticed that at supersonic speeds the sidewash is generally positive since the flow has been forced outward by the nose and the canopy. Near the fusealge lower corner, however, the flow is directed inward because of the effective negative angle of attack. The flow adjacent to the canopy is also inward since the survey plane is behind the position of maximum canopy area.

Results for the angle of attack of 15° indicate local angles of attack generally greater than free stream (i.e., upwash relative to free stream) throughout the flow region surveyed. Upwash angles are greatest near the lower corner of the fuselage where the flow has been accelerated. For supersonic speeds it would be expected that the flow near the body would expand as it negotiates the turn toward the canopy, resulting in higher upwash angles in the upper fuselage corner of the flow region. This was not realized, however, because the canopy shock acts to reduce upwash angles.

For any body at angle of attack, the sidewash is directed outward on the windward side of the fuselage and inward on the lee side. The manner in which this variation from the windward to leeward wides is achieved, however, depends on the Mach number. As can be seen in Fig. 6 the outwash region of the flow field increases slightly with increasing Mach number, primarily because of the increase in the extent of downstream influence of the nose.

The data at 15° angle of attack in Fig. 6 indicate that the total pressure at the forward inlet station is essentially the free-stream value for Mach numbers up to and including 1.8. At the higher Mach number, however, the flow evidently has greater difficulty in negotiating the fuselage corner; consequently, an area of lower total pressure extends into the survey area. The small total pressure defect in the upper fuselage corner of the contour maps at the higher Mach numbers is due to the flow having passed through the canopy shock.

Effects of fuselage lower corner geometry at the forward survey station are illustrated in Fig. 7 for a Mach number of 2.2 and angles of attack of 0° and 15°. Fuselages 1 and 3 are shown to illustrate two variations of corner geometry for a fuselage with a relatively large flat area on the bottom. Fuselages 2 and 4 illustrate the effects for two variations of a corner with a larger average radius of curvature. At 0° angle of attack the predominant effect of a larger corner radius (fuselages 2 and 4) is a slight increase in downwash and greater inwash near the fuselage lower corner. This is expected for all models since the models are effectively at negative angle of attack because of the drooped nose. The flow accelerates downward and inward in turning the fuselage corner; this effect is felt throughout more of the flow field for the larger radius corners.

As can be seen in Fig. 7 for an angle of attack of 15°, the larger radius corner (fuselages 2 and 4) tends to reduce gradients in the flow field associated with flow around the fuselage corner and to increase the flow-field region affected by the corner. Consequently, the inboard lower quadrant of the survey area showed lower Mach numbers, less upwash, and greater sidewash than the fuselages with a sharper corner. The larger corner also eliminated the low total pressures in this quadrant. One curious anomaly exhibited by fuselages 2 and 4, however, is the relatively low total pressure area in the center of the survey region. Reasons for such behavior are unknown at this time, causing some skepticism toward the validity of the data obtained with the center probe in the survey rake. However, no reason other than this unexplained result can be advanced to question the probe measurements.

The effects of the alternate nose and the alternate canopy are shown in Fig. 8 for a Mach number of 2.2 and angles of attack of 0° and 15°. The alternate nose is shorter than the basic nose and has a higher initial angle resulting in a stronger bow shock. At the forward inlet station, however, changes in the flow field due to the alternate nose were practically undiscernible, the only change noted being a slight decrease in total pressure.

The alternate canopy extends farther forward than the basic canopy and has a lower initial inclination angle, which causes a weaker disturbance over more of the surveyed flow field. Being weaker, the disturbance reduces sidewash slightly as may be seen at both 0° and 15° angle of attack in Fig. 8. Differences in downwash caused by the two canopies are insignificant. The most noticeable effect attributable to the alternate canopy may be seen in the total pressure map at $\alpha = 15°$. Evidently the effect of this canopy extends as low as the fuselage corner where the flow interacts with the flow around the corner to reduce total pressure losses in that area of the flow field.

At the aft inlet station located under the wing, the flow field bears little resemblance to the flow at the forward survey plane. This is graphically illustrated in Fig. 9, which shows Mach number effects for fuselage 1 at the aft station at angles of attack of 0° and 15°. Since the wing dominates the flow field, fuselage lower corner effects are of secondary importance; thus the fuselage 1 results are representative of the flow field at the aft inlet location. At $\alpha = 0°$, flow angularities in this survey plane were small for all Mach numbers. The interesting occurrence at $\alpha = 0°$ was the variations in total pressure at the higher Mach numbers. Consequently, total pressure maps are presented on the left-hand side of Fig. 9 to illustrate Mach number effects at 0° angle of attack. A region of low total pressure directly below the wing in the outboard portion of the surveyed area is indicated at $M_\infty = 2.2$. This loss in total pressure is considered to result from the shock off the wing leading edge, since the leading edge is supersonic at this Mach number. Although not shown in Fig. 9, the same phenomenon, corresponding to an almost sonic leading edge occurred at $M_\infty = 1.8$. At $M_\infty = 1.35$ the leading edge is subsonic; consequently, the shock emanating from the wing root is ahead of the survey station, a result borne out by the survey data. Also notable in these contour plots is the accumulation of the boundary layer at the fuselage-wing juncture at $M_\infty = 2.2$.

Due to channeling of the flow in the corner formed by the fuselage and the wing, it would be expected that the flow field at $\alpha = 15°$ would have a downwash equal to the angle of attack at the wing surface, diminishing toward zero at the lower boundary. Similarly, the sidewash angles would be expected to increase with increasing distance from the fuselage. The lower corner of the fuselage would affect the inboard lower quadrant of the flow field and distort the picture somewhat, due to flow from the bottom of the fuselage into the surveyed region. Roughly speaking, just this sort of flow pattern was obtained.

Other phenomena may be recognized from the contour plots of Fig. 9. Evidently the high static pressures under the wing have an adverse effect on the fuselage boundary layer, resulting in a low total pressure area near the fuselage corner. Also recognizable in the total pressure map at $M_\infty = 2.2$ is the same type of disturbance as that seen at $\alpha = 0°$, which is assumed caused by the wing shock. This assumption is given more credence by the flow angularity maps, which indicate approximately free-stream conditions in the lower outboard region of the map. Although not shown in this figure, Mach numbers in this region were also nominally free stream.

7. Concluding Remarks

Immediately obvious from the flow surveys at inlet locations is the diversity of flow fields in which the inlet must operate over the range of Mach numbers and angles of attack. None of the fuselage forebody configurations tested provided the optimum flow fields – a low-distortion flow of high total pressure with little change in Mach number and angle of attack. However, some trends with fuselage geometric variables were noted.

Effects of fuselage lower corner geometry are confined primarily to the lower inboard quadrant of the survey area at the forward inlet station. A corner with a small average radius tends to produce large gradients in flow angularity and local Mach number with some loss in total pressure, whereas a larger average radius tends to reduce these gradients and to distribute them over a larger region of the flow field. Concentration of most of the curvature in the turn toward the bottom of the corner also tends to reduce gradients in the survey area.

The influence of the canopy and nose droop is also indicated at the forward inlet station. At the higher Mach numbers the drooped nose and the canopy combined to cause a downwash and positive sidewash for $\alpha = 0°$, and to reduce the upwash for positive angles of attack. The alternate nose and the alternate canopy generally caused relatively insignificant changes in the flow field. Depending on the relative locations of the canopy and the inlet, however, the flow over the canopy can influence the entire side region and interact with the flow around the fuselage lower corner. For the alternate canopy tested, this interaction improved total pressures near the fuselage corner.

At the aft survey plane the flow field is dominated by the wing. The wing compresses the flow, resulting in relatively high pressures, local Mach numbers less than free stream, and large variations in downwash and sidewash across the survey region. Flow from around the fuselage lower corner into this high pressure region causes an area of low total pressure at the corner extending into the survey field.

8. References

1. Centolanzi, Frank J.: Characteristics of a 40° Cone for Measuring Mach Number, Total Pressure, and Flow Angles at Supersonic Speeds. NACA TN 3967, 1957.

2. Walitt, L., Trulio, J. G., and King, L. S.: A Numerical Method for Computing Three-Dimensional Viscous Supersonic Flow Fields About Slender Bodies. NASA SP-228, 1969, pp. 265-315.

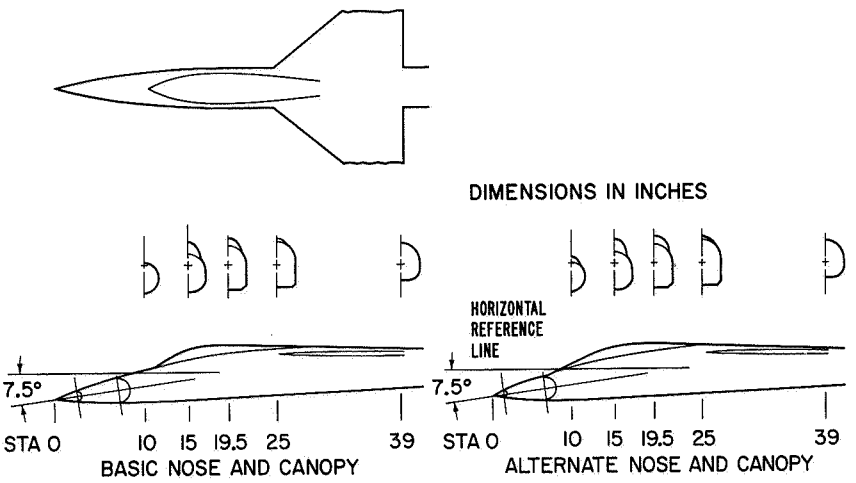

Fig. 1. Typical configuration.

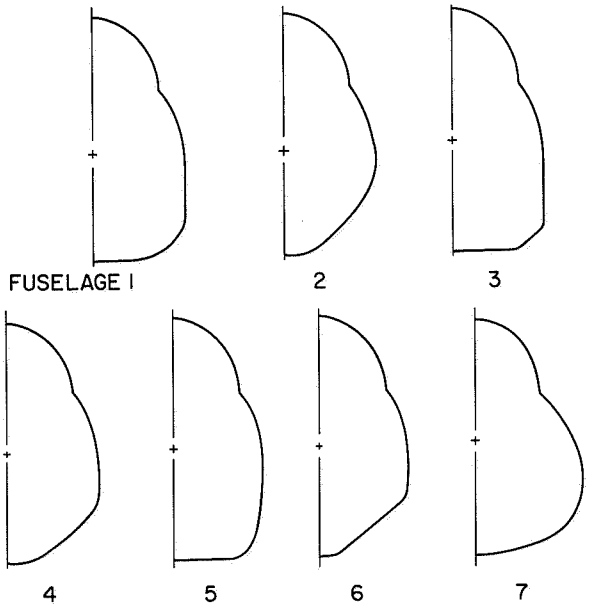

Fig. 2. Sketch of fuselage cross-sectional shapes investigated (sta. 19.5)

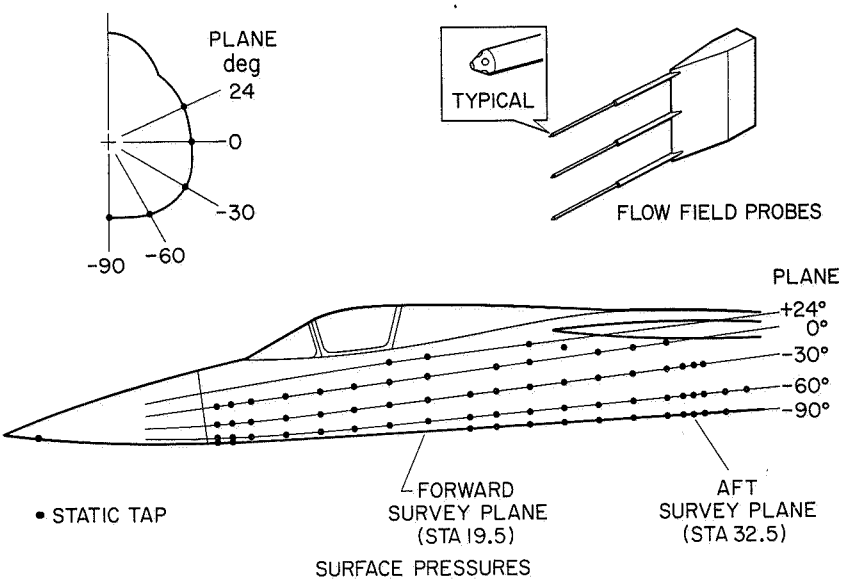

Fig. 3. Instrumentation

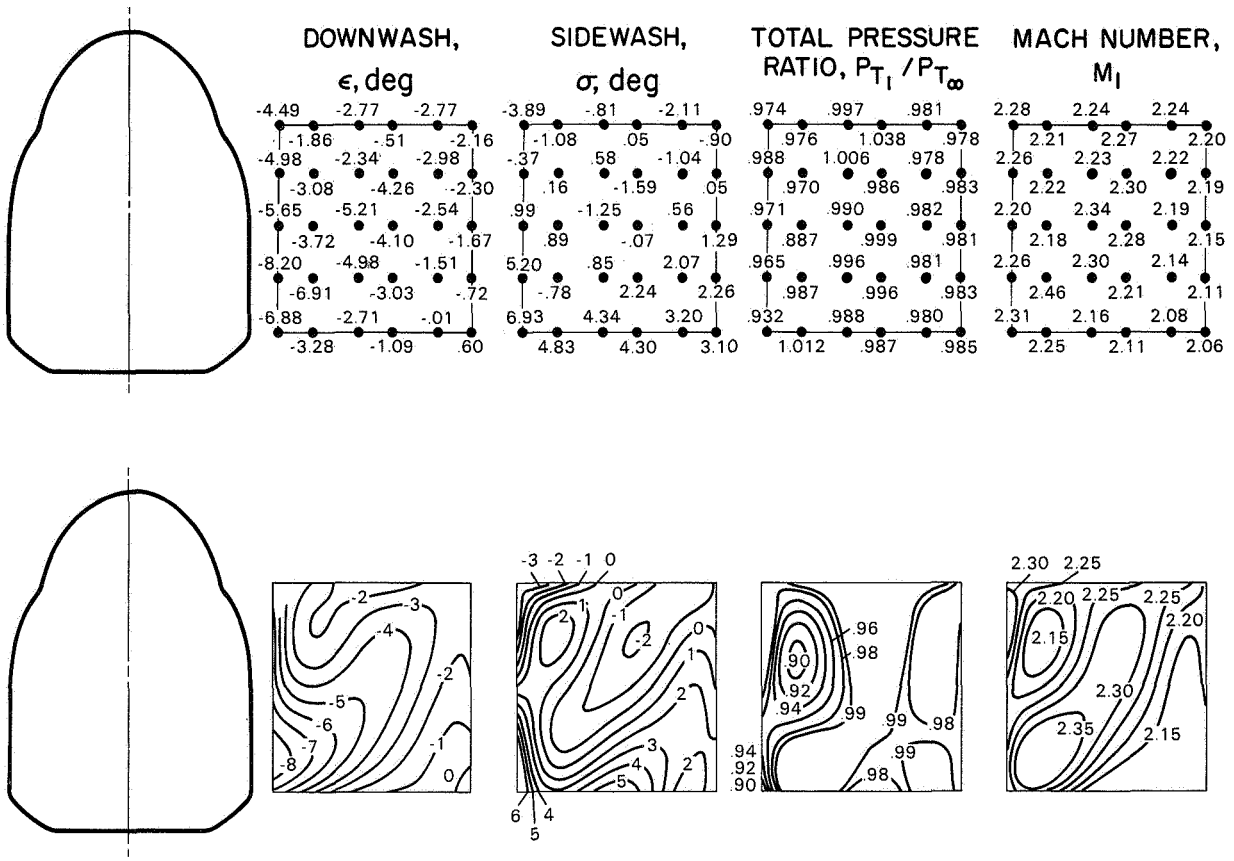

Fig. 4. Comparison of data with computed contours; fuselage 3, $M_\infty = 2.2$, $\alpha = 20.75°$.

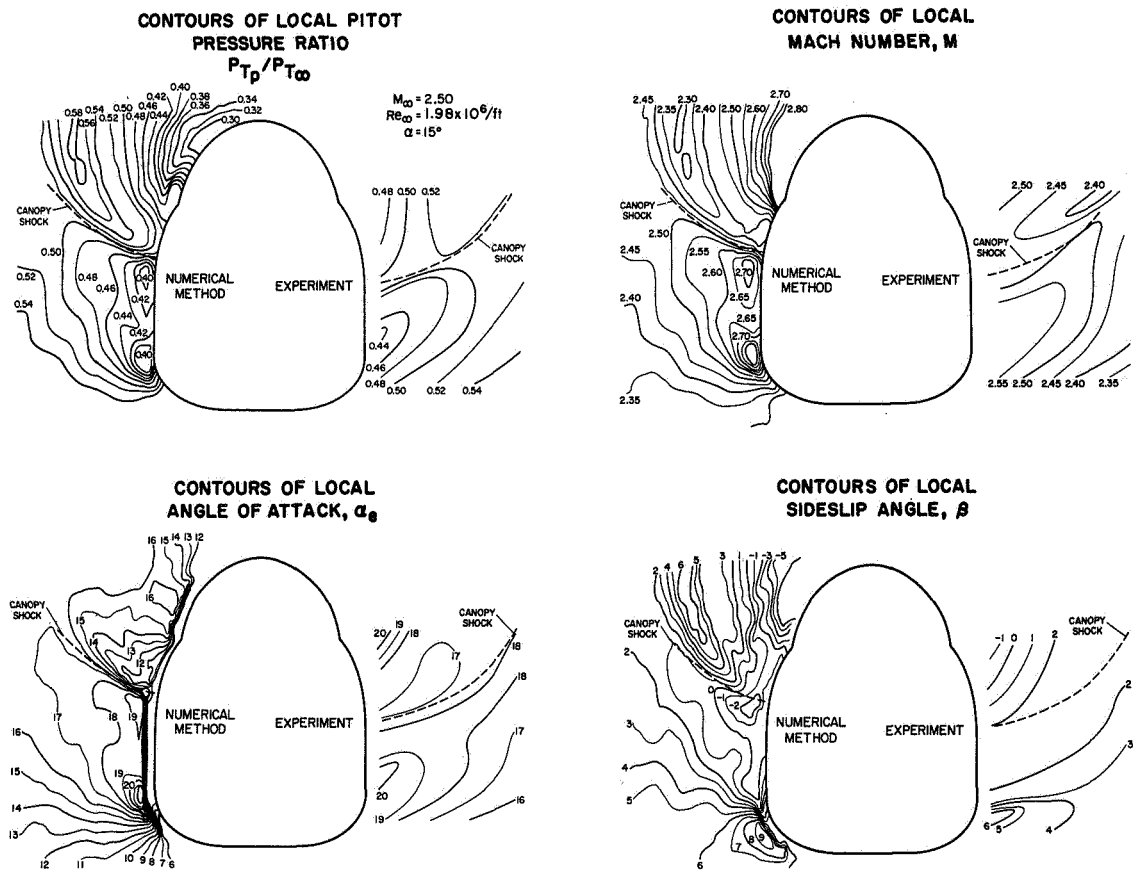

Fig. 5. Comparison of results with numerical method.

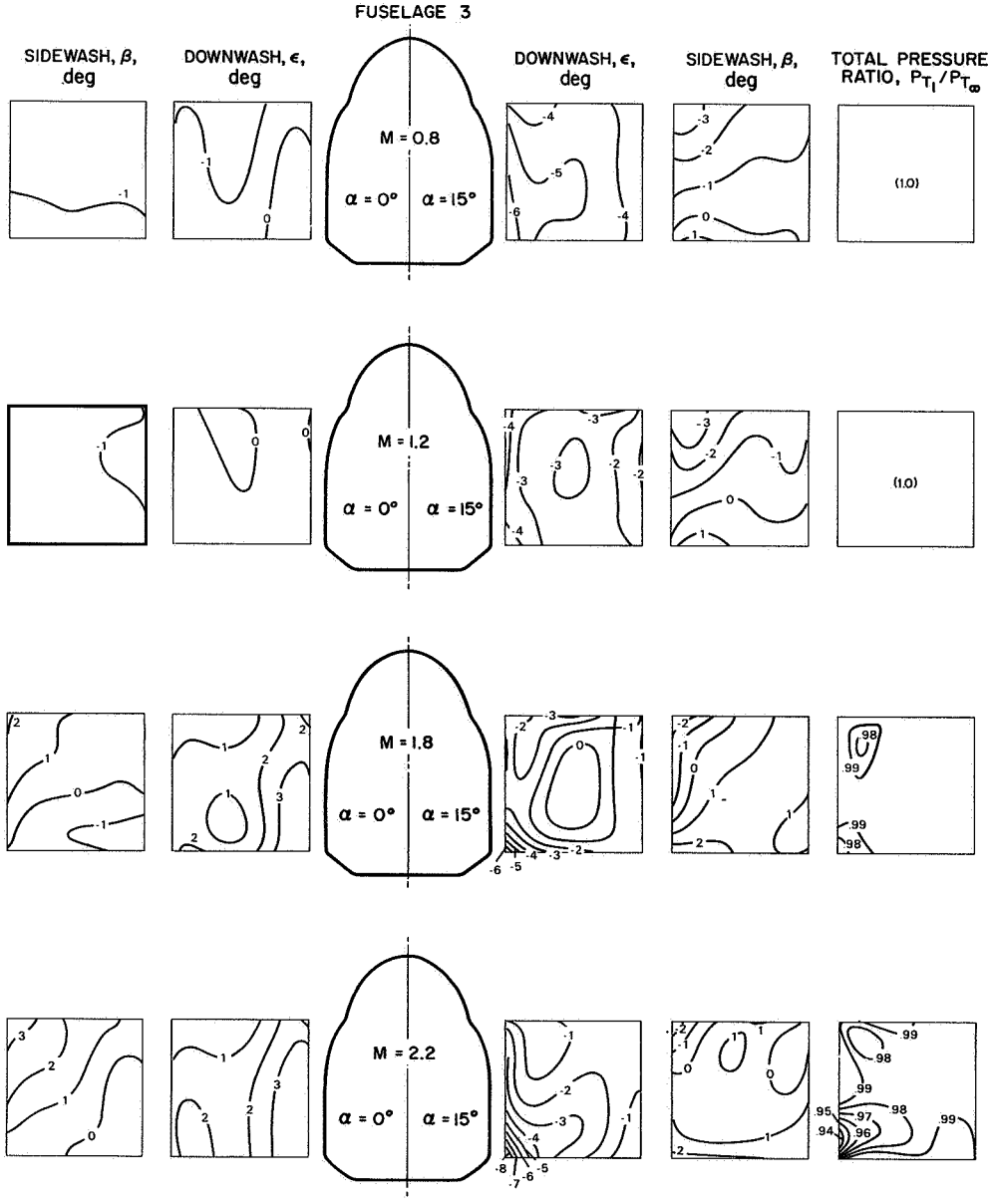

Fig. 6. Mach number effects at forward inlet station.

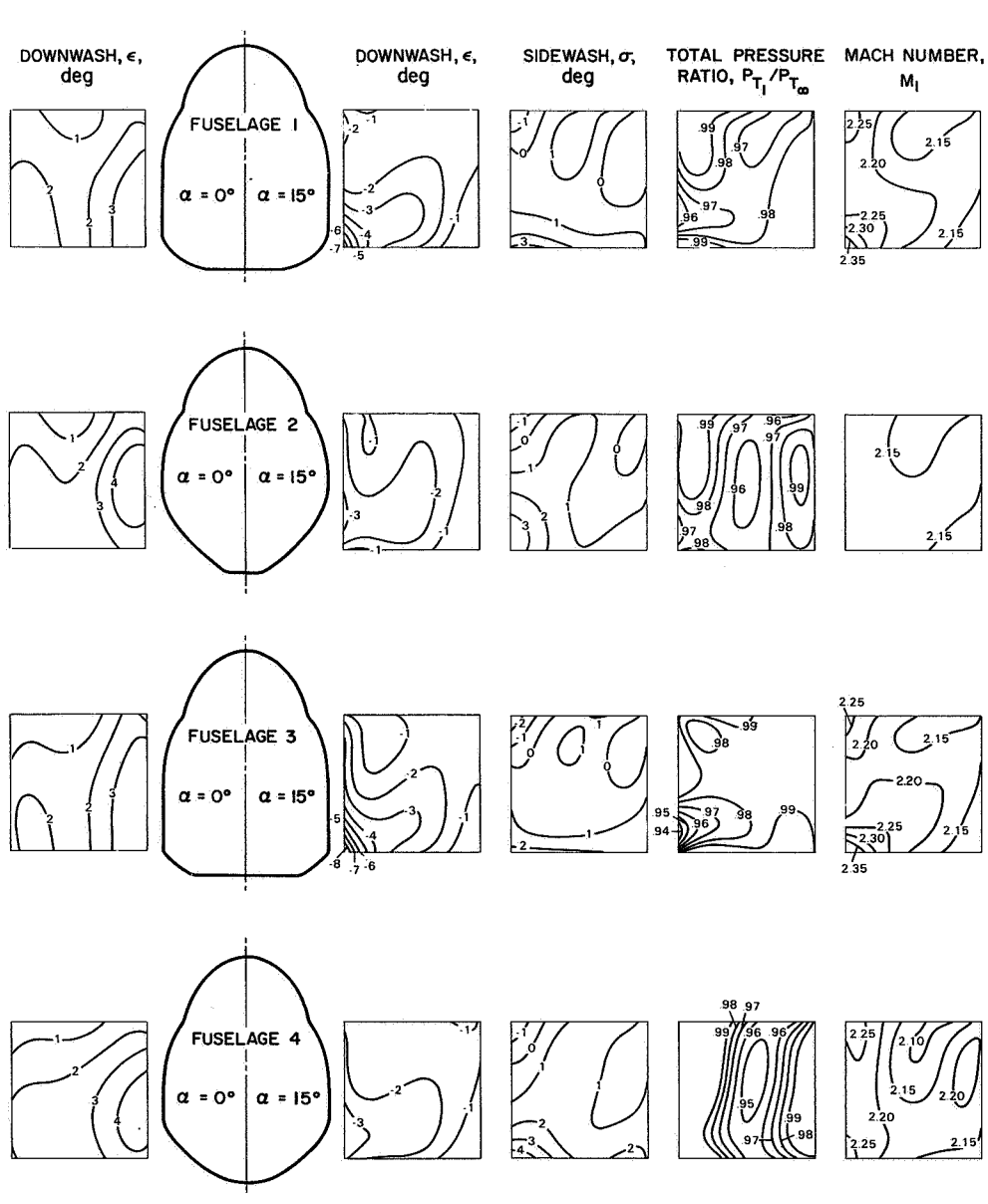

Fig. 7. Fuselage lower corner effects at forward inlet station; $M_\infty = 2.2$.

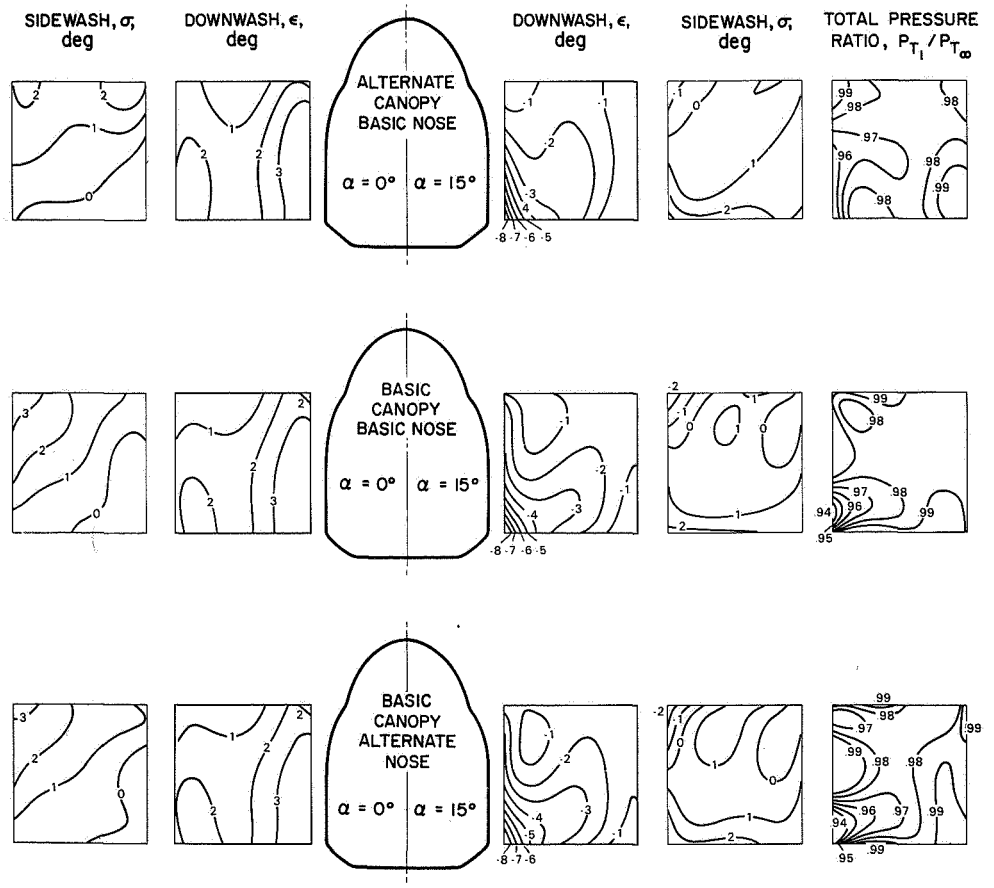

Fig. 8. Nose and canopy effects at forward inlet station; fuselage 3, $M_\infty = 2.2$.

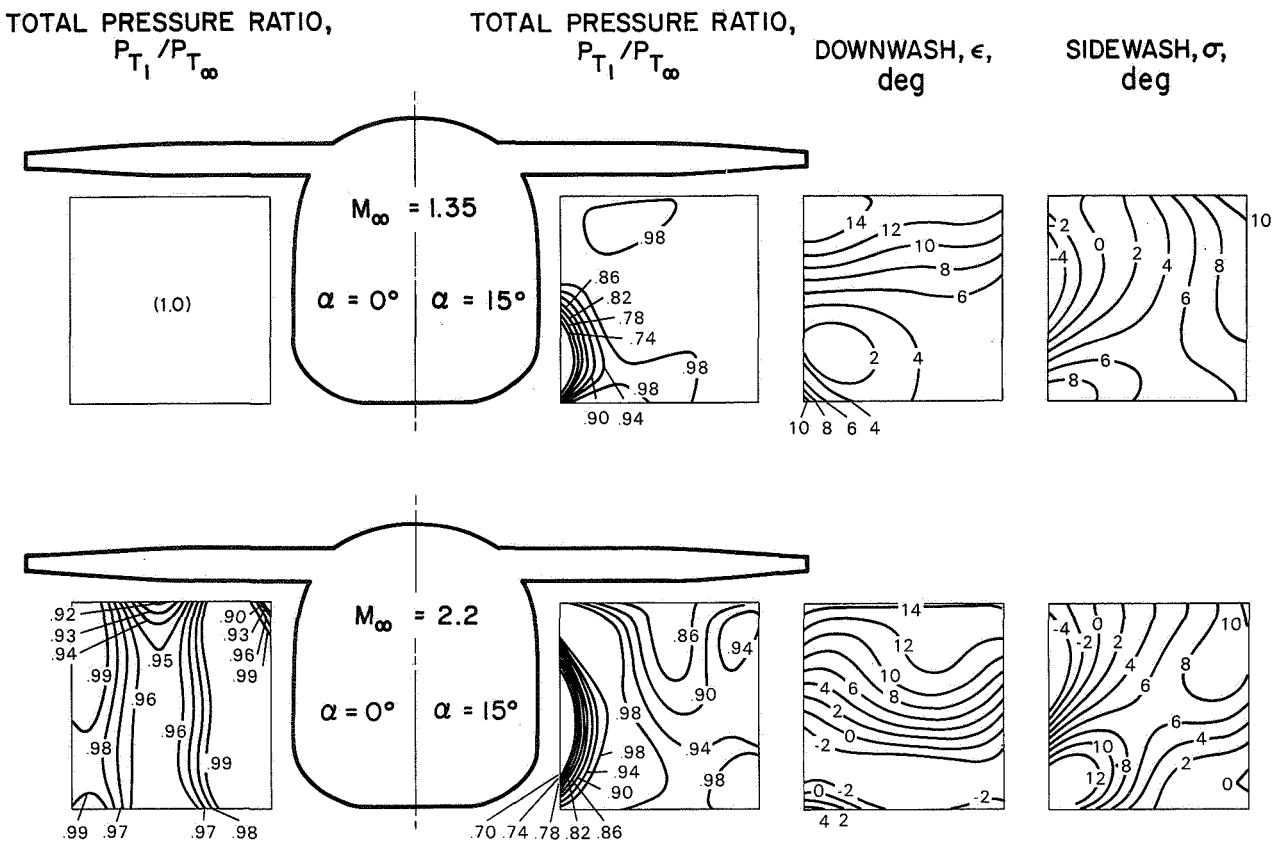

Fig. 9. Mach number effects at aft inlet station; fuselage 1.